# DUSP6 is upregulated in metastasis and influences migration and metabolism in pancreatic cancer cells

Authors: Mariana T. Ruckert[1,2,3], R. McKinnon Walsh[2], Bailey A. Bye[2], Austin E. Eades[2], Wei Yan[4], Filip Bednar[4,5], Jiaqi Shi[5,6], Costas A. Lyssiotis[3,5,7], Michael N. VanSaun[2#], Vanessa S. Silveira[1,8#]

[1]Department of Genetics, Ribeirao Preto Medical School, University of Sao Paulo, Ribeirao Preto, SP, 14040-901, Brazil.

[2]Department of Cancer Biology, University of Kansas Medical Center, Kansas City, KS, 66160, US.

[3]Department of Molecular & Integrative Physiology, University of Michigan, Ann Arbor, MI, 48109, US.

[4]Department of Surgery, University of Michigan, Ann Arbor, MI, 48109, US.

[5]Rogel Cancer Center, University of Michigan, Ann Arbor, MI, 48109, US.

[6]Department of Pathology & Clinical Labs, University of Michigan, Ann Arbor, MI, 48109, US.

[7]Department of Internal Medicine, Division of Gastroenterology and Hepatology, University of Michigan, Ann Arbor, MI, 48109, US.

[8]Massachusetts General Hospital Cancer Center, Krantz Family Center for Cancer Research, Boston, MA; Harvard Medical School, Boston, MA, 02114, US.

Running title: DUSP6 influences migration and glycolysis in PDAC cells.

Keywords: DUSP6; Migration; Glycolysis; Pancreatic cancer; Metastasis.

[#]Corresponding authors: vdasilvasilveira@mgh.harvard.edu, mvansaun@kumc.edu

## ABSTRACT

Pancreatic ductal adenocarcinoma (PDAC) is a highly aggressive malignancy characterized by KRAS mutations in approximately 95% of cases. Despite recent advancements with KRAS inhibitors, therapeutic resistance has emerged, and combination approaches are needed. In particular, it is important to understand how downstream signaling of KRAS supports PDAC growth. For example, DUSP6, a dual-specificity phosphatase that modulates ERK1/2 phosphorylation and RAS pathway activity, has emerged as an important regulator of KRAS-MAPK signaling. Transcriptomic analyses demonstrate that DUSP6 is markedly overexpressed in PDAC tumors compared to non-tumoral pancreatic tissue. Single-cell RNA-seq reveals its upregulation in epithelial tumor cells, with further elevation in metastatic lesions relative to primary tumors. This upregulation correlates with the quasi-mesenchymal/squamous molecular subtype, and clinically, high DUSP6 expression is associated with poorer overall survival. Gene set enrichment analyses of metastatic samples indicate that DUSP6 is linked to pathways involved in cell migration and metabolism. To elucidate DUSP6's functional roles, stable knockdown of DUSP6 in PDAC cell lines resulted in increased ERK/MAPK activation and altered migratory capacity. Metabolic profiling showed enhanced basal glycolysis following DUSP6 suppression. However, combined inhibition of glycolysis and DUSP6 downregulation did not affect the migratory phenotype, indicating that glycolytic alterations do not drive migration. These findings highlight the dual and independent roles of DUSP6 in modulating migratory capacity and glycolysis in PDAC. This study underscores the significance of DUSP6 as a potential therapeutic target and provides new insights into its contributions to PDAC progression.

**SIGNIFICANCE STATEMENT:** DUSP6 plays dual and independent roles in pancreatic cancer, regulating both migration and glycolysis. Its upregulation in metastasis is associated with poor prognosis and more aggressive phenotypes, highlighting its clinical relevance. Targeting DUSP6 represents a potential therapeutic strategy to disrupt KRAS-MAPK signaling and target key pathways driving PDAC progression.

## INTRODUCTION

Pancreatic ductal adenocarcinoma (PDAC) accounts for over 90% of pancreatic cancer cases and is one of the most lethal forms of invasive cancer globally, ranking as the third leading cause of cancer-related mortality [1-3]. Despite significant advancements, the current 5-year survival rate remains low, at 13% [3]. Late detection of PDAC primarily stems from vague symptoms, lack of early diagnostic markers, and resistance to chemotherapy [4, 5]. Complete resection remains the sole curative option, yet it is unattainable for the majority of patients; 80–90% of patients present with locally advanced or metastatic disease upon diagnosis [6, 7]. Metastasis in PDAC commonly affects the liver, peritoneum, and lungs [8-12]. Studies indicate that not all circulating tumor cells successfully initiate secondary tumors, suggesting the requirement for genetic and/or epigenetic changes [13]. Mutations such as those occurring in *Kras* are prevalent in both primary and metastatic tumors, with certain passenger mutations showing a preference for metastatic sites [11, 12]. For example, loss of DPC4 (SMAD4) is more frequent in metastatic cases, correlating with increased invasiveness [14]. Gene expression alterations are also important considerations in this context; however, to date, most studies have only documented changes between non-neoplastic pancreatic and tumor tissues [15].

70 *Kras* mutations are found in approximately 95% of PDAC cases [16] and are the first genetic
71 alterations that arise in precancerous lesions. These mutations alter protein conformation and
72 ultimately lead to a prolonged activation state and, consequently, downstream activation of
73 signaling pathways such as the ERK/MAPK pathway [17]. In tumor cells, ERK
74 phosphorylation drives MYC activation through subsequent phosphorylation, leading to a
75 myriad of effects such as uncontrolled cell proliferation, increased survival, and metabolic
76 rewiring [18, 19]. Although it is intuitive to believe that KRAS constitutive activation is
77 imperative for tumors, its hyperactivation induces oxygen reactive species (ROS) production,
78 and cells are forced to upregulate their antioxidant systems to maintain ROS homeostasis.
79 However, failure to buffer intracellular ROS accumulation can result in oncogene-induced
80 senescence and cytotoxicity [20]. Therefore, fine-tuned KRAS-MAPK activation is required
81 for tumor cells to survive and concurrently evade the detrimental effects of their metabolic
82 adaptations.

83 DUSP6 is a dual-specificity phosphatase that targets serine and threonine residues, particularly
84 dephosphorylating ERK1/2 and downregulating the ERK/MAPK pathway [21]. While DUSP6
85 is reported to act in a negative feedback loop to downregulate ERK/MAPK activation, it has
86 also been reported that ERK1/2 phosphorylates DUSP6 to target this protein for subsequent
87 proteasomal degradation [22]. Its role in cancer is context dependent, acting either as an
88 oncogene or as a tumor suppressor [23]. DUSP6 was previously shown to be upregulated in
89 pancreatic intraepithelial neoplastic (PanIN) lesions (early stage of PDAC tumorigenesis) and
90 downregulated in invasive carcinoma, particularly in poorly differentiated subtypes [24]. This
91 phenomenon has been reported to occur due to hypermethylation of *DUSP6* promoter, leading
92 to abrogation of gene expression and increased activity of the ERK/MAPK pathway [25]. The
93 complex coordination of the KRAS-ERK-DUSP6 axis and the timely regulation of DUSP6

94 expression throughout tumorigenesis prompted us to investigate the role of this molecule in
95 PDAC metastasis.

96 In this study, we demonstrated that *in silico* gene expression and RNAscope studies in human
97 samples revealed upregulation of *DUSP6* in metastatic samples compared to that in primary
98 tumors and non-neoplastic pancreatic tissue. Gene set enrichment analysis (GSEA) of human
99 metastatic PDAC samples revealed enrichment of pathways related to cell migration and
100 metabolism. *In vitro* assessments demonstrated *DUSP6* downregulation in a KRAS mutant
101 cell line, which correlates with increased ERK/MAPK activation, diminished proliferation, and
102 migration capacity; however, this effect was absent in KRAS wild-type cells. Functionally,
103 *DUSP6* downregulation led to elevated basal glycolysis, indicating its involvement in glucose
104 metabolism. However, the combined inhibition of *DUSP6* and glycolysis did not affect the
105 migratory phenotype of the KRAS mutant cell line. Our findings suggest that, while DUSP6
106 influences migration capacity and glucose metabolism, these effects may not be directly
107 correlated in this context.

108

109 **MATERIALS & METHODS**

110 **Cell lines and culture**

111 MIA PaCa-2 (RRID:CVCL_0428), PANC-1 (RRID:CVCL_0480), AsPC-1
112 (RRID:CVCL_0152), BxPC-3 (RRID:CVCL_0186), Capan-2 (RRID:CVCL_0026), and
113 SW1990 (RRID:CVCL_1723) were purchased from the ATCC (Manassas, VA, USA). K8484
114 (RRID:CVCL_XD12) and DT8082 (RRID:CVCL_XD11) were acquired from David
115 Tuveson's laboratory (Cold Spring Harbor Laboratory) [20]. P4313 was acquired from Andy
116 Lowy (UC San Diego) [21]. PKT62 is a murine pancreatic tumor cell line derived from a PKT
117 (*LSL-Kras*$^{G12D/+}$, *TGFBR2*$^{fl/fl}$, *Ptf1a*$^{Cre/+}$) mouse [26] and kindly provided by Michael VanSaun

118 (University of Kansas Medical Center). KPC CAFs and PKT CAFs cell lines were isolated
119 from the respective mouse tumors and validated by western blotting. Briefly, tumors were
120 collected, digested, minced and cells were sorted with EpCAM beads (BioLegend Inc., cat
121 #741444). $EpCAM^-$ cells were kept in culture and until full confluence, protein samples were
122 isolated and fibroblastic phenotype was confirmed by the presence of α-SMA and absence of
123 CK19 and $Ras^{G12D}$. Capan- 2, AsPC-1 and SW1990 were cultured in high glucose (4.5 g/L)
124 RPMI-1640 medium (ThermoFisher Scientific, Waltham, MA USA cat #A1049101)
125 supplemented with 10% heat-inactivated fetal bovine serum (FBS, Atlanta Biologicals/RD
126 Systems, Atlanta, GA USA) and antibiotic-antimycotic (Thermo Fisher Scientific cat#
127 15240062). The K8484 cell line was cultured in high-glucose (4.5 g/L) Dulbecco's Modified
128 Eagle Media (Thermo Fisher Scientific, cat# 11-995-073) supplemented with 5% heat-
129 inactivated FBS (R&D Systems-Atlanta Biologicals) and antibiotic-antimycotic (Thermo
130 Fisher Scientific). All other cell lines were maintained in high-glucose DMEM supplemented
131 with 10% FBS and antibiotic-antimycotic. Cells were maintained in culture conditions (37°C,
132 5% $CO_2$ and humid atmosphere) as recommended by the ATCC, utilized within 15 passages
133 from purchase and regularly tested for mycoplasma.

134 **Plasmids and gene knockdown**

135 To generate *DUSP6* knockdown cells, short hairpin RNA (shRNA) constructs targeting three
136 independent regions of DUSP6 mRNA (#1 5'-CTGTGGTGTCTTGGTACATTG-3'; #2 5'-
137 TCTAATCCAAAGGGTATATTT-3,' #3 5'-ATTCGGCATCAAGTACATCTT-3') were
138 obtained from Millipore (Burlington, MA, USA). The empty vector pLKO.1 puro
139 (RRID:Addgene_8453) was used as a control. Packaged lentiviruses were generated by
140 transfecting HEK293T (RRID:CVCL_0063) cells with the respective plasmids and the Trans-
141 Lentiviral™ Packaging Mix (Open Biosystems) to produce viral supernatants, which were
142 subsequently concentrated with Lenti-X™ concentrator (TakaraBio, cat #631231). Next,

143 $2.5x10^5$ pancreatic cancer cells were seeded in 6-well plates and incubated for 24h with
144 lentiviral suspension. Successfully transduced cells were selected with puromycin treatment
145 (1-2.5µg/mL) until complete cell death was achieved in the non-transduced cells.

146 **RNA isolation and RT-qPCR**

147 Briefly, $10^6$ cells were seeded in 6-well plates and incubated overnight. The next day, cells
148 were washed with 1X PBS and harvested using QIAzol Lysis Reagent (Qiagen, GmbH, cat
149 #79306). Samples were stored at -80°C until total RNA was isolated using the Direct-zol RNA
150 Miniprep kit (Zymo Research Corporation), according to the manufacturer's protocols. RNA
151 quantification and quality analyses were performed using NanoDrop 2000 (Thermo Fisher
152 Scientific Inc.). For cDNA, 1.5-2µg of RNA was processed using the High-Capacity cDNA
153 Reverse Transcription Kit (Applied Biosystems, cat #4368814) according to the
154 manufacturer's instructions. The product was further diluted 1:10 before storage at -20°C.
155 Real-time PCR analysis was carried out with the 2X SYBR Green qPCR Master Mix (ApexBio
156 Technology, cat #K1070) on a ViiA 7 Real-Time PCR System (Applied Biosystems) using the
157 following primers: human *DUSP6* (Fwd: ATGGTAGTCCGCTGTCCAAC/Rev:
158 ACGTCCAAGTTGGTGGAGTC), mouse *Dusp6* (Fwd: TGTTTGAGAATGCGGGCGAGTT
159 / Rev: ACAGTTTTTGCCTCGGGCTTCA), human *ACTB* (Fwd:
160 TCGTGATGGACTCCGGTGAC/Rev: CGTGGTGGTGAAGCTGTAG), and mouse *Actb*
161 (Fwd: GTGACGTTGACATCCGTAAAGA / Rev: GCCGGACTCATCGTACTCC). Each
162 sample was run in triplicate using the $2^{-\Delta\Delta CT}$ method (Livak & Schmittgen, 2001) and the fold-
163 change was evaluated relative to normal samples and determined using *ACTB/Actb* levels as a
164 reference.

165 **Western blotting**

166 Briefly, $10^6$ cells were plated in 6-well plates, incubated overnight, and collected the next day
167 for protein isolation. Cells were washed with 1X PBS, lysed in ice-cold RIPA buffer (1X RIPA
168 [Cell Signaling Technology]; 10mM NaF; 1mM PMSF), sonicated, and incubated on ice for
169 10 min. The cells were then centrifuged at 16,000 × *g* for 10 min at 4°C. Protein quantification
170 was performed using the Pierce™ BCA Protein Assay Kit (Thermo Fisher Scientific),
171 following the manufacturer's instructions. For western blotting assays, 10 µg of total protein
172 was loaded in each lane of a 10% polyacrylamide gel and subjected to electrophoresis. Proteins
173 were transferred to nitrocellulose membranes using the semi-dry method on a Trans-Blot Turbo
174 Transfer System (Bio-Rad). Specific proteins were detected using the following primary
175 antibodies: P-ERK1/2 (Cell Signaling Technology, cat #4370, RRID:AB_2315112, link),
176 ERK1/2 (Cell Signaling Technology, cat #4695, RRID:AB_390779, link), E-cadherin (Cell
177 Signaling Technology, cat #3195, RRID:AB_2291471, link), N-cadherin (Cell Signaling
178 Technology, cat #13116, RRID:AB_2687616, link), and β-actin (Cell Signaling Technology,
179 cat #12262, RRID:AB_2566811, link) and MKP-3 (Santa Cruz Biotechnology, cat #sc-
180 137246, RRID:AB_2095347, link). Secondary antibodies used were Peroxidase AffiniPure
181 $F(ab')_2$ Fragment Donkey Anti-Mouse IgG (H+L) (cat #715-036-151, RRID:AB_2340774,
182 link) and Donkey Anti-Rabbit IgG (H+L) (cat #711-036-152, RRID:AB_2340590, link) from
183 Jackson ImmunoResearch Laboratories Inc. Images were obtained using FluorChem M (Bio-
184 Techne) or a Sapphire FL Biomolecular Imager (Azure), and analyzed using ImageJ software
185 (NIH, Bethesda, MD, USA).

186 **Immunohistochemistry staining**

187 Healthy pancreata, primary tumor, and metastatic samples were collected from wild-type
188 C57BL/6J (RRID:IMSR_JAX:000664) mice, *LSL-Kras*$^{G12D/+}$, *Ptf1a*$^{Cre/+}$ (KC), *LSL-Kras*$^{G12D/+}$,
189 Tp53$^{R172H/+}$, *Ptf1a*$^{Cre/+}$ mouse pancreatic tissue (KPC) maintained in a C57BL/6J background.
190 Male and female mice were used for experiments and mice ages varied from 5.9 to 86.6 weeks.

191 Samples were collected, embedded in paraffin, and sectioned into 4μm sections. The paraffin
192 sections were processed as follows: 15 min in xylene (2x); 5 min in 100% ethanol (2x) and 5
193 min in 75% ethanol. Finally, the sections were washed 3x in PBS at room temperature (RT).
194 Antigen retrieval was performed by boiling the sections in 10 mmol/L sodium citrate solution
195 for 10 min and waiting for the sections to cool down and achieve RT. Next, the sections were
196 washed 3x with PBS, quenched with 3% $H_2O_2$ for 15 min, and blocked with 5% BSA for 20
197 min. Whole-slide scanning was performed using a PANNORAMIC Scan II scanner
198 (3DHISTECH). Immunohistochemical staining was performed by iHisto Inc. (Salem MA;
199 iHisto.io) using an anti-DUSP6 antibody (Abcam, cat #ab76310, RRID:AB_1523517, link).
200 Ten fields per independent section from each condition were randomly selected for
201 quantification using the QuPath software [27]. The study weas performed under protocols
202 2005N000148 and 2019N000116 approved by the IACUC at MGH, and at Pharmaron Inc. and
203 Champions Oncology under approved protocols.

204 **RNA *in situ* hybridization**

205 RNA in situ hybridization was performed using the RNAscope® technology (Advanced Cell
206 Diagnostics, Inc.). Briefly, tumors were collected from the mice, sectioned, and immediately
207 fixed in 10% buffered formalin for 24h. Tumor sections were preserved in 70% ethanol,
208 embedded in paraffin blocks, cut into 5 μm sections, and placed in pre-treated slides. The
209 sections were freshly cut for the assay and dried at RT to preserve RNA integrity. Sections
210 were baked for 1h at 60°C and then deparaffinized using Histo-Clear (Electron Microscopy
211 Science, cat #6411004) and 100% ethanol. Next, sections were treated with RNAscope®
212 Hydrogen Peroxide for 10 min at RT, followed by a target retrieval step with RNAscope® 1X
213 Target Retrieval Reagent for 15 min, and finally, RNAscope® Protease Plus treatment for 30
214 min at 40°C. Finally, we used the RNAscope® 2.5 HD Duplex Reagent Kit, following the
215 manufacturer's protocol. Specific probes used in this assay were Mm-Dusp6 (cat #429321-C1),

216 Mm-Krt19-C2 (cat #402941- C2) and Mm-Pdgfrb-C2 (cat #411381-C2). The sections were
217 imaged at 20x magnification using an EVOS™ M5000 Imaging System (Thermo Fisher
218 Scientific).

219 **Clinical samples**

220 All the human patient samples described in this study were collected from patients undergoing
221 pancreas resection due to pancreatitis, cystic neoplasms or PDAC from 2002 to 2015 at the
222 University of Michigan Health System. Collection of these samples was approved by the
223 Institutional Review Board at the University of Michigan (IRB number: HUM00098128).

224 **RNA *in situ* hybridization combined with immunofluorescence multiplex staining**

225 Tissue microarray (TMA) sections were obtained, set up and processed as described in [28].
226 Fluorometric in-situ hybridization was performed according to the manufacturer's (Advanced
227 Cell Diagnostics, Inc.) instructions. Briefly, FFPE preserved TMAs were cut in 5 µm sections,
228 and placed in pre-treated slides. Sections were freshly cut for the assay and dried at RT to
229 preserve RNA integrity. Sections were baked for 1h at 60°C, deparaffinized in xylene three
230 times for 15 mins, washed in 100% ethanol twice for 3 mins and air dried. Slides were treated
231 with pretreatment 1, 2 and 3 buffers, rinsed in double-distilled water (dd$H_2O$) and incubated
232 with the DUSP6 (cat #1032061-C1) or control probes for 2h at 40°C in a humidity chamber.
233 Slides were then treated with Amp solutions 1-6 before the fluorogenic substrate Opal 690 TSA
234 (Akoya Biosciences, Inc.) was applied to the slide. After a 10 min incubation, the slides were
235 washed and then subjected to dual immunofluorescent staining on a Ventana Discovery Ultra
236 stainer (Roche Diagnostics, North America) with smooth muscle actin (BioCare Medical, cat
237 #001, RRID:AB_2910606, link, 1:100, 60 mins, Opal 570) and pan-cytokeratin (Abcam, cat
238 #ab9377, RRID:AB_307222, link, 1:200, 20 mins, Opal 520). Slides were mounted using
239 Prolong Gold with DAPI and scanned using a Vectra Polaris™ (Akoya Biosciences, Inc.)

240 whole slide scanner. Images were analyzed using the de-array TMA tool in QuPath and DAPI
241 was used to identify individual cells in each core.

242 **Proliferation assay**

243 Cell proliferation was assessed by ethynyldeoxyuridine (EdU) incorporation. Briefly, 2.5-
244 5x$10^4$ cells were seeded in 24-well plates in complete media and incubated overnight. The next
245 day, the media was replaced with the appropriate treatments and incubated for 18 h. At this
246 point, EdU was added to the wells at a final concentration of 10µM and cells were incubated
247 for an additional 6h. At the end of this period, the cells were trypsinized, harvested, and fixed
248 with 10% buffered formalin overnight at 4°C with gentle agitation. The next day, the cells were
249 washed with PEB-T (1x PBS, 2mM EDTA, 1% BSA, 0.5% Triton-X) and subsequently with
250 PB (1x PBS, 1% BSA). Next, the cells were resuspended in Click-It Reaction ($H_2O$, 100mM
251 Tris pH 8.5, 1mM $CuSO_4$, 1µM azide-dye) and 100mM ascorbic acid. Cells were incubated
252 with 0.5µg/mL propidium iodide (PI), washed twice, and resuspended in PEB (1x PBS, 2mM
253 EDTA, 1% BSA) for flow cytometry analysis. The cells were analyzed for 530 nm and 695 nm
254 emission using an Attune NxT Flow Cytometer (Thermo Fisher Scientific). FCS files were
255 analyzed with FlowJo™ v10.8 Software (BD Biosciences) and the percentage of EdU-positive
256 cells was taken from the PI-positive single cells.

257 **Migration assay**

258 First, 2-4x$10^5$ cells were seeded into 24-well plates and cultured until they reached full
259 confluence. Then, a scratch was made at the center of the plate using a 200µL pipette tip. Wells
260 were washed twice with 1X PBS to discard all debris, and media with appropriate treatments
261 were added. The plates were photographed at 0 and 24h using an EVOS™ M5000 Imaging
262 System (Thermo Fisher Scientific). Scratch area was calculated using the Wound Healing
263 Coherency Tool (Montpellier Ressources Imagerie) on ImageJ (NIH, Bethesda, MD,

264 RRID:SCR_003070, link) and results are expressed as healing percentage – the difference in
265 scratch area between time 0 and time 24.

266 ***In silico* analysis**

267 *DUSP6* expression analysis was performed using publicly available datasets obtained from The
268 Cancer Genome Atlas (TGCA_PAAD), Genotype-Tissue Expression (GTEx, normal
269 pancreatic tissue) and Gene Expression Omnibus (GEO, RRID:SCR_005012, link; GSE62452
270 [29], GSE28735 [30], GSE15471 [31], GSE71729 [32] and GSE224564 [33]). Overall
271 survival analysis was performed by Gene Expression Profiling Interactive Analysis (GEPIA,
272 RRID:SCR_018294, link) using the UCSC Xena project (http://xena.ucsc.edu) datasets.
273 Differential expression of *DUSP6* in the epithelial and stromal compartments was performed
274 using GSE93326 [34] with the R2 Genomics Analysis and Visualization Platform. The latter
275 was also utilized for accession of Bailey *et al.* [35] dataset since ICGC Data Portal Repository
276 was discontinued. Finally, *DUSP6* expression was correlated with Metastatic Potential
277 (MetMap 500 [36]) at the DepMap Portal using the Cancer Cell Line Encyclopedia (CCLE).
278 We specifically filtered the cell lines for Exocrine Adenocarcinoma, which corresponds to
279 PDAC cell lines. Gene set enrichment analysis was conducted in a cohort of metastatic samples
280 from the publicly available dataset GSE71729 [32] using the hallmark gene set collection
281 (version 2024) available at GSEA 4.3.3. software (RRID:SCR_003199, link) [37]. Single-cell
282 analysis was performed using a previously published [38] pancreatic tissue single-cell atlas
283 (link).

284 **Glycolysis stress test**

285 Glycolysis rates were determined using the Seahorse XF Glycolysis Stress Test Kit (Agilent,
286 Santa Clara, CA, USA), following the manufacturer's protocol. Briefly, 2-4x$10^4$ cells were
287 seeded into a 96-well plate and incubated overnight. The next day, cells were washed twice

288 with Seahorse XF DMEM (pH 7.4 (2mM glutamine) and a final volume of 180µL of the same
289 was added to each well. The extracellular acidification rate (ECAR) was measured (mpH/min)
290 at 11 time points with sequential injections of 10mM Glucose, 1µM Oligomycin and 100mM
291 2-Deoxy-D-glucose (Thermo Scientific, cat. #AC111980010). For nuclear staining, 5µg/mL
292 Hoechst was added to the oligomycin solution. The ECAR values were calculated and
293 normalized to the cell count number using an automated imaging and cell counting workflow.
294 For normalization, the ECAR value per $10^3$ cells was set, and the Agilent Seahorse XF system
295 automatically calculated and generated normalized results.

296 **Lactate assay**

297 For lactate measurement, $2.5 \times 10^4$ cells were seeded in 96-well plates and allowed to sit
298 overnight in the incubator. The next day, the complete media in the plate was replaced with
299 new media containing 0.5% FBS, and the cells were incubated for 24h. At the end of the
300 experiment, culture plates were centrifuged at 450 × *g* for 5 minutes and 10µL of media was
301 collected from each well for the subsequent assay. For lactate quantification, we utilized the
302 Glycolysis Cell-Based Assay Kit (Cayman Chemical Company, Ann Arbor, MI, USA, cat
303 #600450), following the manufacturer's protocol. The absorbance was read at 490 nm using a
304 Synergy H1 Multimode microplate reader (Bio-Tek/Agilent Technologies).

305 **Statistical analysis**

306 Sample sizes were chosen to achieve a minimum of triplicate samples for all the experiments.
307 For the assessment of statistical significance between two groups, Welch's t-test was used for
308 parametric data, while Mann-Whitne test was used for non-parametric data. For comparison
309 across multiple groups, Brown-Forsythe and Welch ANOVA test or mixed-effects analysis
310 with Šídák's multiple comparisons test were used when appropriate for parametric data; for
311 non-parametric data, Kruskal-Wallis test were performed. Data normality was determined

312 based on Q-Q plots distribution. All statistical tests were performed using GraphPad Prism 9
313 software (RRID:SCR_002798, link), and the results were considered significant at $\alpha = 0.05$. *
314 $P < 0.05$, ** $P < 0.01$, *** $P < 0.001$, and **** $P < 0.0001$.

315 **RESULTS**

316 ***DUSP6* overexpression is correlated with advanced stage PDAC.**

317 To investigate the role of DUSP6 in metastasis, we first confirmed its expression in tumor
318 samples. To evaluate *DUSP6* expression in PDAC samples, we used three distinct in silico
319 datasets available on public platforms (GSE62452 [29], GSE28735 [30] and TCGA/GTEx).
320 Our analysis revealed that *DUSP6* was upregulated in primary tumor samples compared to non-
321 tumoral pancreatic tissue across all analyzed datasets (Figure 1A-C). Based on these findings,
322 we aimed to assess *DUSP6* expression in metastatic cases. Utilizing the *in silico* dataset
323 GSE71729 [32], we compared *DUSP6* expression across a cohort comprising 134 non-tumor
324 tissue samples, 145 primary tumor samples, and 62 metastatic samples derived from various
325 secondary sites. Notably, we observed that *DUSP6* was significantly overexpressed in
326 metastatic samples compared to both primary tumor samples ($P < 0.0001$) and non-tumorous
327 pancreatic tissue (Figure 1D). Considering that *DUSP6* is overexpressed in primary tumors and
328 metastatic samples, we hypothesized that there is a possible correlation between DUSP6
329 expression and patient prognosis. To answer this question, we first assessed its expression in
330 the PDAC molecular subtypes. We performed *in silico* analysis utilizing PDAC molecular
331 subtyping [35, 39]. We took advantage of the datasets from Badea *et al.* (GSE15471) and
332 Bailey *et al.* [35] and analyzed *DUSP6* expression in distinct PDAC subtypes. In the Badea *et*
333 *al.* cohort (Figure 1E), we observed that *DUSP6* was overexpressed in the quasi-mesenchymal
334 subtype compared to non-tumoral pancreatic tissue ($P < 0.0001$) and the exocrine-like subtype
335 ($P = 0.0211$). Likewise, in the Bailey *et al.* cohort (Figure 1G), we observed DUSP6

336 overexpression in the squamous subtype compared to that in the pancreatic progenitor (P =
337 0.0065) and immunogenic (P = 0.0197) subtypes. Next, we performed the same analysis using
338 another subtyping paradigm [32]; however, no differences were observed (Figure 1F). The
339 same subtyping was used to stratify samples in the GSE224564 [33] (Figure 1H) dataset, and
340 we observed overexpression of *DUSP6* in the basal-like subtype compared to the classical
341 subtype (P = 0.0292). The quasi-mesenchymal, squamous, and basal-like subtypes share
342 similar molecular signatures and worse prognoses than the other PDAC subtypes. Collectively,
343 these results suggest that DUSP6 is enriched in this tumor phenotype. To establish a link
344 between DUSP6 expression and ERK1/2 activation, we performed a correlation analysis
345 between *DUSP6* expression and *MAPK1* expression in quasi-mesenchymal samples from
346 GSE15471 [31]. We observed a moderate positive correlation in this context (R = 0.6787, P =
347 0.02), suggesting that DUSP6 overexpression may be required to counteract MAPK signaling
348 (Figure S1A).

349 Supporting the latter, our analysis of TCGA dataset revealed that high *DUSP6* expression in
350 PDAC patients correlated with worse overall survival (P = 0.0058; Figure 1I). Despite the
351 counterintuitive nature of *DUSP6* overexpression in metastatic samples, given the prevailing
352 dogma suggesting its negative regulation of the ERK/MAPK pathway, our findings were
353 substantiated by further correlation analysis conducted with 30 PDAC cell lines from the
354 Cancer Cell Line Encyclopedia (CCLE) and the Metastasis Map (MetMap 500 [36]). This
355 analysis revealed a moderate positive correlation between *DUSP6* expression and metastatic
356 potential in these cell lines (R = 0.611; P = 0.0003; Figure 1J). Furthermore, this correlation
357 analysis indicated that *DUSP6* gene expression ranked as the eighth strongest positive
358 correlation for metastatic potential within this PDAC cell line cohort among a list of 1000 genes
359 (Figure 1K). Collectively, these observations suggest that *DUSP6* overexpression in PDAC

360 samples is associated with the poorest prognostic outcomes and correlates with progression to
361 metastasis.

362 To validate these findings, we assessed DUSP6 expression in lesions across different stages of
363 the disease using healthy murine pancreatic tissue, primary tumors, and liver metastasis
364 samples. We observed a trend of temporal control of DUSP6 expression with disease
365 progression, although the results were not statistically significant (Figure 2A). DUSP6
366 expression is upregulated during the acinar-to-ductal metaplasia (ADM) process and
367 subsequently reduced in pancreatic intraepithelial neoplastic (PanIN) lesions. DUSP6 was
368 again increased in primary tumor lesions and, finally, in liver metastasis samples. These results
369 suggest that temporal control of DUSP6 expression is differentially utilized during PDAC
370 tumorigenesis and progression, perhaps to fine-tune MAPK signaling.

371 PDAC has a highly complex microenvironment and is mainly composed of dense
372 fibroinflammatory stroma consisting predominantly of activated stromal fibroblasts and
373 immunosuppressive immune cell types. Our previous analyses were primarily performed on
374 bulk tumors, where gene expression represents a composite of myriad cell types in the tumor
375 microenvironment. Accordingly, we assessed whether DUSP6 overexpression was localized to
376 specific cell types within the tumor. To answer this question, we examined *DUSP6* expression
377 in different tumor compartments using GSE93326 [34]. Indeed, our analysis revealed that
378 *DUSP6* was significantly upregulated in tumor cells compared to stromal cells ($P < 0.0001$;
379 Figure S1B). We validated this analysis by assessing DUSP6 protein levels in four mouse
380 PDAC cell lines and two mouse cancer-associated fibroblast (CAF) cell lines. The mouse cell
381 lines exhibited varying levels of the protein, with DT8082 and K8484 demonstrating the
382 highest DUSP6 levels, P4313 showing intermediate levels, and PKT62 displaying the lowest
383 levels (Figure S1C). Subsequently, we investigated *Dusp6* expression in mouse tumor tissue
384 using RNA in situ hybridization (RNA-ISH) technology. We examined *Dusp6* mRNA levels

385 in tumor sections obtained from *LSL-Kras*$^{G12D/+}$, *Ptf1a*$^{Cre/+}$ (KC), *LSL-Kras*$^{G12D/+}$, Tp53$^{R172H/+}$,
386 *Ptf1a*$^{Cre/+}$ (KPC) mice, co-stained for either *Krt19* (a tumor epithelial cell marker) or *Pdgfrb* (a
387 stromal marker). As depicted in Figure 1SC, *Dusp6* (green dots) exhibited strong co-expression
388 with *Krt19* (red dots, upper images), but not with *Pdgfrb* (red dots, lower images), in both
389 genetic backgrounds. Consistent with the western blot analysis of protein levels, both KC and
390 KPC pancreata demonstrated *Dusp6* overexpression in malignant epithelial cells, whereas
391 stromal compartment expression remained low (Figure S1D). To further explore the link
392 between DUSP6 expression and MAPK signaling, we leverage GSE93326 [34] to perform a
393 correlation analysis between *DUSP6* and *MAPK1* in the epithelial and stromal compartments.
394 Interestingly, we observed a moderate positive correlation in gene expression levels in the
395 epithelial compartment ($R = 0.6105$, $P < 0.0001$) but not in the stromal compartment ($P =$
396 $0.0321$, $P = 0.789$) in this cohort (Figure S1E-F). Altogether, these data indicate that DUSP6
397 is upregulated in PDAC epithelial cells in the context of hyperactivated MAPK signaling.

398 To confirm whether these observations could be translated into human disease, we used a panel
399 of human samples from two TMAs containing normal pancreatic tissue/pancreatitis, intraductal
400 papillary mucinous neoplasms (IPMN), mucinous cystic pancreatic neoplasms (MCN), PanIN,
401 PDAC, and PDAC metastasis. We differentially stained tissue compartments with duplex
402 RNA-ISH specific markers using panCK for epithelial cells and αSMA for CAFs (Figure 2C).
403 A general assessment of *DUSP6* positive cells throughout the cores revealed a trend similar to
404 that observed in mouse tissue. Although not statistically significant, we observed a slight
405 decrease in expression in PDAC primary tumors compared to that in normal pancreatic tissue
406 and a subsequent increase in metastatic samples (Figure 2D). Furthermore, we observed a
407 significant increase in *DUSP6* expression in epithelial cells throughout tumor progression, and
408 once again, a notable decrease in *DUSP6* expression in PDAC primary tumors, followed by

409 upregulation in metastatic samples (Figure 2E). These findings suggest that *DUSP6* timely
410 upregulation is required for metastatic tumor cells in the foreign environment.

411 The observation that *DUSP6* expression is significantly lower in PDAC primary tumor cells is
412 counterintuitive, considering what we previously observed in bulk RNA-seq datasets.
413 Considering these previous observations and the complexity of the PDAC microenvironment,
414 we decided to dig further into a publicly available pancreatic tissue single-cell atlas [38] to
415 characterize *DUSP6* expression patterns in different cell types within the healthy donor
416 pancreas, adjacent normal pancreatic tissue, and primary tumor microenvironment. Figure 2F
417 depicts the UMAP plot of all the cell types identified in the bulk of human patient samples.
418 Interestingly, we observed that regardless of the context, DUSP6 was majorly expressed in
419 myeloid cells, with increased expression in macrophages (Figures 2G-I, Figure S2A).
420 Nevertheless, when we look specifically at the epithelial cells, in these three contexts, we
421 observe a 2.4-fold increase in the percentage of *DUSP6* expressing epithelial cells in PDAC
422 compared to healthy pancreata (Figure S2A). Lastly, we performed co-expression analysis of
423 *DUSP6* and *KRT19* and confirmed a 1.8 × increase in *DUSP6* positive cells in PDAC *KRT19*
424 positive cells compared to healthy pancreata (Figure 2J). These results support *DUSP6*
425 upregulation in epithelial cells within the tumor microenvironment. Interestingly, *in silico*
426 analysis utilizing a bulk RNAseq dataset from Bojmar *et al.* [40] reveals that *DUSP6* is
427 upregulated in liver biopsy samples from patients who eventually developed PDAC liver
428 metastasis in comparison to those who did not in a 3-year follow up study (Figure S2B). Our
429 results also indicate a role for DUSP6 in the immune cell compartment, which may explain the
430 variations in DUSP6 expression observed in different PDAC human samples when evaluated
431 through bulk RNA sequencing. Additionally, DUSP6 expression may influence the
432 establishment of the pre-metastatic niche.

433 ***DUSP6* expression in metastatic samples correlates with decreased oxidative**
434 **phosphorylation and increased glycolysis.**

435 To gain further insight into the functional significance of *DUSP6* overexpression in metastatic
436 samples, we aimed to elucidate the pathways involved. To accomplish this, we revisited the
437 GSE71729 [32] dataset and conducted gene set enrichment analysis using 62 metastatic
438 samples. Intriguingly, our analyses revealed enrichment of several pathways associated with
439 cell motility, epithelial-to-mesenchymal transition, and metabolism. Notably, these
440 enrichments revealed a positive correlation between *DUSP6* expression and cell migration
441 (Figure 3B), suggesting an upregulation of this process, along with a negative correlation
442 between its expression and oxidative phosphorylation (Figure 3A), suggesting a
443 downregulation of this pathway. Supporting these observations, Panther Pathway enrichment
444 analyses conducted across two independent datasets (TCGA_PAAD and CPTAC_PDAC)
445 highlighted Glycolysis (P00024) as one of the pathways most strongly correlated with *DUSP6*
446 expression in PDAC across all three datasets (Table S1). Moreover, other enrichment analyses
447 utilizing the CPTAC Protein dataset indicated a correlation between DUSP6 protein levels and
448 the Pentose phosphate pathway (P02762), Glucose 6-phosphate metabolic process
449 (GO:0051156), and Carbon metabolism (hsa01200) (Table S1). These findings prompted us to
450 hypothesize that *DUSP6* overexpression may play a pivotal role in metabolic reprogramming
451 of tumor cells during metastasis.

452 ***DUSP6* downregulation reduces proliferation and migration in PDAC cell lines.**

453 Considering *DUSP6* upregulation in metastatic samples, we performed *DUSP6* knockdown in
454 PDAC cell lines exhibiting the highest levels of the protein, one of which was derived from
455 metastatic ascites (AsPC-1, Figure S3A). *DUSP6* knockdown was confirmed through gene
456 expression and protein level analyses (Figure 3D, S3). As expected, *DUSP6* knockdown led to

457 increased activation of ERK1/2, as confirmed by enhanced phosphorylation on western blotting
458 (Figure 3D). Subsequently, considering that ERK1/2 activation elicits a proliferative
459 phenotype, we evaluated cell proliferation using ethynyldeoxyuridine (EdU) incorporation
460 assays under conditions of full serum (5%) and serum deprivation, designed to either stimulate
461 or inhibit proliferation. Surprisingly, both AsPC-1 and BxPC-3 cell lines exhibited impaired
462 proliferation after *DUSP6* knockdown. Notably, AsPC-1 cells displayed a more pronounced
463 decrease, particularly under serum-starved conditions ($P < 0.0001$; Figure S4A). While BxPC-
464 3 cells also showed significant proliferation impairment ($P < 0.0001$), they were less affected
465 by serum starvation compared to AsPC-1 cells (Figure S4B).

466 To confirm our prior observations in human samples, we investigated the impact of *DUSP6*
467 knockdown on cell migratory capacity. *In vitro* migration assays conducted within 24h of
468 scratching (time 0) revealed distinct phenotypes among the cell lines. AsPC-1 cells exhibited
469 a significant reduction in migratory capacity upon DUSP6 knockdown ($P < 0.0001$; Figure
470 S4C), whereas BxPC-3 cells showed no significant effect (Figure S4D).

471 In summary, our findings suggest that DUSP6 plays a role in regulating both proliferation and
472 migration capacity of PDAC cells, albeit with potential context-dependent differences.

473 ***DUSP6* downregulation increases glycolytic flux in PDAC cell lines.**

474 To ascertain DUSP6's involvement in tumor cell metabolism, we first evaluated basal lactate
475 secretion in extracellular media following *DUSP6* knockdown using a colorimetric assay. In
476 this context, distinct phenotypes were observed in both cell lines: BxPC-3 cells exhibited a
477 significant increase in lactate secretion compared to the control ($P < 0.0001$), whereas AsPC-1
478 cells showed no significant difference compared to the control (Figure 3F).

479 Considering that glucose is the primary source of energy for tumor cells *in vitro*, we sought to
480 delineate how DUSP6 affects glucose metabolism in each cell line and conducted a metabolic

481 assay to measure glycolysis activity in the absence of *DUSP6* (Figure 3E). Upon *DUSP6*
482 knockdown and glucose injection, both AsPC-1 and BxPC-3 cells demonstrated a statistically
483 significant increase in basal glycolysis (Figure 3G), consistent with observations from the
484 lactate secretion assay. Following treatment with oligomycin, an inhibitor of ATP synthase
485 (complex V), which shuts down mitochondrial respiration and makes cells dependent on
486 glycolysis for ATP production, we observed a significant increase in glycolytic capacity in
487 AsPC-1 cells upon *DUSP6* knockdown compared to the control ($P < 0.05$; Figure 3H), with no
488 significant differences in glycolytic reserve (Figure 3I). This indicates that the absence of
489 *DUSP6* alone leading to pronounced ERK1/2 activation pushes these cells towards their
490 maximum glycolytic potential. Upon the addition of 2-DG, glycolysis was completely
491 abolished under all conditions. These results demonstrate that *DUSP6* inhibition affects
492 glycolysis in PDAC under basal metabolic conditions, but subsequent rescue experiments are
493 required to determine the observed changes in glycolytic reserve.

494 **Glycolysis inhibition does not provide an additional impact cell migratory capacity in**
495 ***DUSP6* depleted cells.**

496 To gain deeper insights into how metabolic changes induced by *DUSP6* knockdown affect cell
497 behavior, we conducted a cell proliferation assay. By reducing fetal bovine serum in the media
498 to minimize its metabolic influence, we assessed cell proliferation with and without 2-DG
499 addition. Consistent with our previous findings, both AsPC-1 and BxPC-3 cells exhibited a
500 significant reduction in proliferation upon *DUSP6* knockdown compared to their respective
501 controls. Following 2-DG treatment, BxPC-3 cells displayed a notable decrease in proliferation
502 under both conditions, with the reduction being more pronounced in the control cells ($P <$
503 $0.0001$; Figure S5B). In contrast, AsPC-1 showed no discernible effect on proliferation
504 compared to the same conditions without 2-DG (Figure S5A).

505 Subsequently, to establish a link between the metabolic phenotype and metastatic potential of
506 these cells, we conducted a migratory capacity assay combined with 2-DG treatment. *DUSP6*
507 knockdown significantly reduced the migratory capacity of AsPC-1 cells, whereas no change
508 was observed in BxPC-3 cells (Figure S4). Unexpectedly, treatment with 2-DG did not
509 significantly alter the migratory phenotype observed in AsPC-1 cells, but significantly reduced
510 BxPC-3 migratory capacity upon DUSP6 knockdown (Figure 3J-K). Interestingly, we noted
511 that in the presence of an external source of pyruvate in the media, the cells maintained their
512 glycolytic potential, even when treated with electron transport chain (ETC) inhibitors
513 (Rotenone and Antimycin A) and 2-DG (Figure S5C). This suggests that pyruvate availability
514 plays a critical role in the decision to sustain aerobic glycolysis or to feed the TCA cycle. These
515 findings suggest that, under nutrient-rich conditions, both AsPC-1 and BxPC-3 utilize different
516 energy sources for migration.

517 **DISCUSSION**

518 DUSP6 is differentially expressed during PDAC tumorigenesis and progression [24]. However,
519 little is known about the role of phosphatases in the development and establishment of
520 metastasis. Our group observed that *DUSP6* was overexpressed in primary tumor samples
521 compared to non-tumoral pancreatic tissues by analyzing *in silico* datasets and spatial transcript
522 profiling. To further investigate the complex feedback loops involving DUSP6 and the
523 ERK/MAPK signaling pathway, we evaluated *in silico* data to assess *DUSP6* expression in
524 late-stage PDAC samples. We observed that *DUSP6* was overexpressed in metastatic samples
525 compared to primary tumor samples by leveraging *in silico,* immunohistochemistry, and
526 multiplex RNAscope analysis. Translational relevance for *DUSP6* expression was observed in
527 survival data; TCGA analysis showed that high DUSP6 expression correlates with lower
528 overall survival in PDAC patients. Finally, when we analyzed *DUSP6* expression among
529 different PDAC molecular subtypes [35, 39], *DUSP6* overexpression was pronounced in the

530 quasi-mesenchymal/squamous subtype, which is associated with a worse prognosis [41]. These
531 data support the hypothesis that *DUSP6* overexpression confers a more aggressive phenotype,
532 further impacting metastasis and worsening overall survival in PDAC.

533 Spatial localization is critical for investigating the functionality. Through *in silico* analysis of
534 pancreatic tumor samples, we determined that *DUSP6* expression was upregulated in the
535 epithelial compartment of the tumor rather than in the stromal compartment. The same pattern
536 was observed in mouse models assessing protein presence by immunohistochemistry and RNA
537 *in situ* hybridization in mouse pancreatic tumors. In human samples, we observed a significant
538 decrease in *DUSP6* expression in PDAC epithelial cells versus normal pancreatic tissue, but
539 increased expression in metastatic epithelial cells. By leveraging a single-cell RNA-seq Human
540 Pancreatic Cancer Atlas, we were able to confirm that *DUSP6* expression is increased in PDAC
541 epithelial cells. However, the results also highlighted macrophages as a subset of cells with
542 important changes in *DUSP6* expression throughout tumorigenesis. Kidger *et al.* recently
543 reported similar RNA *in situ* hybridization results using KC mice, demonstrating that *DUSP6*
544 expression is found in ductal cells in PanINs, but not in stromal cells [42]. Our results
545 confirmed that PDAC tumor cells overexpress *DUSP6*, suggesting the need for further
546 investigation of its role in tumor development.

547 Previous studies on multiple tumor types have linked high DUSP6 expression to worse
548 prognosis and metastasis [43-45]. *DUSP6* has alternatively been described as a tumor
549 suppressor gene in PDAC. Furukawa *et al.* reported that downregulation of *DUSP6* coordinated
550 PDAC progression via hypermethylation of its promoter [24, 25]. Kidger *et al.* also proposed
551 a tumor suppressor role for *Dusp6*, observing that KCD6$^{-/-}$ animals develop a higher number
552 of poorly differentiated tumors and liver metastases [42]. In their model, *Dusp6* was
553 constitutively absent, leading to a permanent state of Erk1/2 activation, which would
554 predictably result in more aggressive tumors and more metastatic foci. Our current hypothesis

555 is that *DUSP6* suppression might allow tumor initiation, while its expression is required for
556 metastatic cells to re-establish in a new environment. Reinforcing this idea, *DUSP6*
557 overexpression appears to correlate with the more invasive quasi-mesenchymal subtype.

558 To investigate this, we subjected PDAC cell lines to stable *DUSP6* knockdown and evaluated
559 their proliferation and migration capacities. Surprisingly, we did not find consensus regarding
560 the observed phenotypes. All statistically significant changes in proliferation indicated an
561 impairment in this capacity. This observation is counterintuitive because it is widely known as
562 a dogma in the field that ERK1/2 activation leads to increased cell proliferation. However, it is
563 also known that tumor cells require fine-tuning of ERK1/2 activation, in which too much
564 MAPK signaling can bypass the fitness advantage and become detrimental to cell growth [46].
565 Similarly, Gutierrez-Prat *et al.* recently reported that depletion of DUSP4, another ERK1/2
566 negative regulator, reduces proliferation by driving "oncogene overdose" in BRAF- and
567 NRAS-mutant melanoma cell lines [47]. The migration phenotype varied among the cell lines,
568 complicating any definitive conclusions on this topic. We hypothesized that this variability
569 might be due to natural compensatory mechanisms within the cells, resulting from dependence
570 on this signaling pathway. AsPC-1 cells carry two alleles of the $KRAS^{G12D}$ mutation, which is
571 the most commonly found among PDAC patients and, therefore, more clinically relevant.
572 BxPC-3 cells present with wild-type *KRAS* which might explain the differences observed
573 between these two cell lines. A recent study by Bulle *et al.* showed that upon MAPK
574 pharmacological inhibition, *DUSP6* is one of the top downregulated genes, demonstrating that
575 *DUSP6* expression correlates with ERK/MAPK activation. Supporting this evidence, we
576 observed that *DUSP6* was significantly upregulated in tumor cell lines harboring a *KRAS*
577 mutation compared to tumor cells driven by other mutations in the CCLE dataset (Figure S6).
578 Bulle *et al.* also demonstrated that upon MAPK inhibition, DUSP6 was targeted for
579 proteasomal degradation, leading to an increase in HER2 activation [48]. Interestingly, this is

580 the first time that DUSP6 has been described as a negative regulator of HER2, since it was
581 previously thought to be ERK-specific. This discovery shifts the paradigm of DUSP6's
582 functional role and raises the possibility that it may be involved in the negative feedback for
583 other signaling pathways. Additionally, it is important to consider that DUSP6 is not the only
584 phosphatase acting as a regulator of ERK phosphorylation. Therefore, its downregulation may
585 elicit compensatory responses from other molecules, ultimately offsetting its absence. Ito and
586 colleagues recently demonstrated a co-dependence of DUSP4 and DUSP6 in MAPK-pathway-
587 driven tumors as a mechanism of drug resistance [49]. In this regard, we highlight that many
588 DUSPs, among other proteins, are involved in ERK1/2 negative feedback control and have
589 been shown to act synergistically to prevent oncogene-induced senescence [23]. Similarly, we
590 found a positive correlation between DUSP6 and MAPK1 expression in tumor cells, but not in
591 stromal cells, in a human cohort, suggesting that these cells are also dependent on DUSP6 for
592 ERK1/2 modulation; we cannot, however, rule out the involvement of other DUSPs in the
593 process. Moreover, the BxPC-3 cell line does not harbor a *KRAS* mutation, and thus, its
594 tumorigenic behavior does not rely on this condition. The observed phenotype in this cell line
595 might be driven by mechanisms different from those initially hypothesized. Conversely, the
596 AsPC-1 cell line, a metastatic PDAC line harboring a *KRAS* mutation, more closely mimics the
597 genetic background that we aimed to investigate. In this cell line, we observed a significant
598 impairment in migration capacity upon *DUSP6* knockdown and increased ERK1/2 activation.

599 To understand the mechanisms by which *DUSP6* affects the metastatic potential of PDAC cells,
600 we performed gene set enrichment analysis using the metastatic cohort of samples from the
601 GSE71729 [32] dataset. This analysis indicated a positive correlation with cell migration and
602 a consistent negative correlation with oxidative phosphorylation. Consequently, we conducted
603 a glycolysis stress test and observed that the absence of *DUSP6* led to increased glycolytic
604 function in PDAC cell lines. This upregulation of glycolysis was confirmed by the increased

605 extracellular acidification rate upon glucose supplementation (in the absence of pyruvate),
606 which could be completely reversed by the addition of 2-DG. This shift towards a more
607 glycolytic phenotype was expected based on previous literature showing that *KRAS*$^{G12D}$
608 increases glucose uptake and glycolytic flux through MAPK activation in PDAC cells: Ying
609 and colleagues demonstrated that increased glycolytic flux induces the non-oxidative pentose
610 phosphate pathway (PPP), which is involved in processes such as nucleic acid synthesis and is
611 closely related to cell proliferative capacity [18]. However, in this context, we observed that
612 although glycolysis was induced upon *DUSP6* knockdown, the cells showed a decreased
613 proliferative capacity, a phenotype that is consistent among the cell lines. This behavior might
614 be linked to inherent differences in cell metabolism among PDAC cell lines, as it has been
615 previously reported that cells can present distinct metabolic profiles despite their growth rates
616 [50]. Interestingly, Hsu *et al.* have demonstrated that DUSP6 is required for T-cell receptor-
617 mediated glycolysis, and that in the absence of DUSP6, T cells show higher dependence on
618 glutamine and fatty acids to fuel the TCA cycle [51]. These findings reinforce DUSP6's
619 involvement in metabolic reprogramming but highlight the context-dependency of the
620 observed phenotypes.

621 Finally, we hypothesized that the induction of glycolysis through *DUSP6* inhibition would
622 decrease the migratory potential of these cells, which could be rescued by the addition of 2-
623 DG, leading to irreversible glycolysis inhibition. We treated the cells with 2-DG and evaluated
624 their migratory capacity but did not observe significant changes with the combination of
625 *DUSP6* and glycolysis inhibition. Previous studies have demonstrated that the induction of
626 glycolysis leads to increased metastatic potential due to the promotion of epithelial-to-
627 mesenchymal transition (EMT) [52, 53]. In the present study, we demonstrated that while cells
628 acquire a more glycolytic phenotype upon *DUSP6* inhibition, their migratory capacity is
629 abrogated. However, inhibition of glucose flux failed to rescue the observed phenotype. We

630 hypothesized that, in a context where pyruvate is available in the culture media, cells can
631 bypass 2-DG-mediated glycolysis inhibition. To estimate the effect of glycolysis induction on
632 the metastatic behavior of *DUSP6* knockdown cells, it is recommended to closely control
633 nutrient availability in the media. While it is tempting to extrapolate our observations to the
634 decreased metastatic potential of the cells, we must reiterate that metastasis encompasses a
635 variety of complex processes involving both intrinsic and extrinsic signals [54]. To further
636 understand DUSP6's role in metastatic potential, it will be necessary to explore other
637 mechanisms involved in metastasis, such as invasive potential and the ability of these cells to
638 adapt to a new environment, which is highly correlated with their metabolic reprogramming
639 capacity.

640 **CONCLUSIONS**

641 This study provides new insights into the role of DUSP6 in PDAC metastasis and metabolism.
642 We demonstrated that DUSP6 inhibition elicits cell-specific effects on migratory potential,
643 while inducing glycolysis in PDAC cells. However, we were unable to establish a direct
644 correlation between the two processes. Future studies should include *in vivo* metastatic assays
645 upon DUSP6 inhibition, as well as metabolomic analysis, to better understand how PDAC cells
646 reprogram their metabolism in the absence of DUSP6 to thrive and survive in a secondary
647 niche.

648 **ACKNOWLEDGEMENTS**

649 We would like to acknowledge Dr. David Tuveson (CRUK) for supplying the murine K8484
650 cell line used in these studies: Dr. Andrew Lowy (UCSD) for supplying the P4313 cell line;
651 Dr. Dafydd Thomas, at the Research Histology and Immunohistochemistry Core (University
652 of Michigan), for conducting the RNA-ISH multiplex assay; the Merchant Lab (University of
653 Miami) for use of the PKT62 cell line; and the Flow Cytometry Core Laboratory at KUMC,

which is sponsored, in part, by the NIH/NIGMS COBRE grant P30 GM103326 and the NIH/NCI Cancer Center Grant P30 CA168524.

## FINANCIAL SUPPORT

This study was supported by São Paulo Research Foundation (FAPESP 2015/10694-5) granted to VSS. MTR was supported by CAPES Foundation (Finance Code 001) and Fulbright Association. JS is supported in part by the National Cancer Institute of the National Institutes of Health under award number R37CA262209. MVS received funds from the University of Kansas Cancer Center. CAL was supported by the NCI (R37CA237421, R01CA248160, and R01CA244931).

## AUTHOR'S CONTRIBUTIONS

MTR: methodology, data collection, formal analysis, visualization, paper writing, and editing; RMW: data collection, formal analysis, and editing; BBB, AEE, WY, FB, JS: data collection and analysis; CAL: supervision, methodology, data analysis, editing; MNV: supervision, methodology, data analysis, paper writing, and editing; VSS: funding acquisition, project administration, conceptualization, supervision, methodology, data analysis, paper writing, and editing.

## COMPLIANCE WITH ETHICAL STANDARDS

All experiments involving mice were approved by the Ethics Committee on Animal Research at Ribeirao Preto Medical School, University of São Paulo (protocol# 016/2018), and were conducted in accordance with the Guidelines of the Brazilian College of Animal Experimentation.

## CONFLICTS OF INTEREST

676 In the past three years, CAL has consulted for Astellas Pharmaceuticals, Odyssey Therapeutics,
677 Third Rock Ventures, and T-Knife Therapeutics, and is an inventor on patents pertaining to
678 Kras regulated metabolic pathways, redox control pathways in pancreatic cancer, and targeting
679 the GOT1-ME1 pathway as a therapeutic approach (US Patent No: 2015126580-A1,
680 05/07/2015; US Patent No: 20190136238, 05/09/2019; International Patent No:
681 WO2013177426-A2, 04/23/2015).

682

683 **REFERENCES**


684 1. Wood, L.D. and R.H. Hruban, *Pathology and Molecular Genetics of Pancreatic*
685 *Neoplasms.* Cancer journal (Sudbury, Mass.), Nov-Dec 2012. **18**(6).
686 2. Muñoz, A.R., et al., *Pancreatic cancer: Current status and Challenges.* Current
687 pharmacology reports, 2017/12. **3**(6).
688 3. Siegel, R.L., A.N. Giaquinto, and A. Jemal, *Cancer statistics, 2024.* CA: A Cancer
689 Journal for Clinicians, 2024/01/01. **74**(1).
690 4. Bardeesy, N., et al., *Pancreatic cancer biology and genetics.* Nature Reviews Cancer
691 2002 2:12, 2002/12. **2**(12).
692 5. McGuigan, A., et al., *Pancreatic cancer: A review of clinical diagnosis, epidemiology,*
693 *treatment and outcomes.* World Journal of Gastroenterology, 2018/11/11. **24**(43).
694 6. Vincent, A., et al., *Pancreatic cancer.* Lancet (London, England), 2011/08/08.
695 **378**(9791).
696 7. Rawla, P., T. Sunkara, and V. Gaduputi, *Epidemiology of Pancreatic Cancer: Global*
697 *Trends, Etiology and Risk Factors.* World Journal of Oncology, 2019/02. **10**(1).
698 8. Disibio, G. and S.W. French, *Metastatic patterns of cancers: results from a large*
699 *autopsy study.* Arch Pathol Lab Med, 2008. **132**(6): p. 931-9.
700 9. Kamisawa, T., et al., *Hematogenous metastases of pancreatic ductal carcinoma.*
701 Pancreas, 1995. **11**(4): p. 345-9.
702 10. Mao, C., et al., *Observations on the Developmental Patterns and the Consequences of*
703 *Pancreatic Exocrine Adenocarcinoma.* Archives of Surgery, 1995/02/01. **130**(2).

704 11. Embuscado, E.E., et al., *Immortalizing the complexity of cancer metastasis: genetic*
705 *features of lethal metastatic pancreatic cancer obtained from rapid autopsy.* Cancer
706 Biol Ther, 2005. **4**(5): p. 548-54.
707 12. Yachida, S. and C.A. Iacobuzio-Donahue, *The pathology and genetics of metastatic*
708 *pancreatic cancer.* Arch Pathol Lab Med, 2009. **133**(3): p. 413-22.
709 13. Haeno, H., et al., *Computational modeling of pancreatic cancer reveals kinetics of*
710 *metastasis suggesting optimum treatment strategies.* Cell, 2012. **148**(1-2): p. 362-75.
711 14. Wilentz, R.E., et al., *Loss of expression of Dpc4 in pancreatic intraepithelial neoplasia:*
712 *evidence that DPC4 inactivation occurs late in neoplastic progression.* Cancer Res,
713 2000. **60**(7): p. 2002-6.
714 15. CA, I.-D., *Genetic evolution of pancreatic cancer: lessons learnt from the pancreatic*
715 *cancer genome sequencing project - PubMed.* Gut, 2012 Jul. **61**(7).
716 16. Hayashi, A., et al., *The pancreatic cancer genome revisited.* Nature Reviews
717 Gastroenterology & Hepatology 2021 18:7, 2021-06-04. **18**(7).
718 17. EA, C., et al., *A central role for RAF→MEK→ERK signaling in the genesis of*
719 *pancreatic ductal adenocarcinoma - PubMed.* Cancer discovery, 2012 Aug. **2**(8).
720 18. Ying, H., et al., *Oncogenic Kras Maintains Pancreatic Tumors through Regulation of*
721 *Anabolic Glucose Metabolism.* Cell, 2012/04/04. **149**(3).
722 19. Than, M.T., et al., *KRAS-Driven Tumorigenesis and KRAS-Driven Therapy in*
723 *Pancreatic Adenocarcinoma.* Molecular Cancer Therapeutics, 2024/10/01. **23**(10).
724 20. N, D. and S. P, *Targeting reactive oxygen species in development and progression of*
725 *pancreatic cancer - PubMed.* Expert review of anticancer therapy, 2017 Jan. **17**(1).
726 21. Alonso, A., et al., *Protein tyrosine phosphatases in the human genome.* Cell, 2004.
727 **117**(6): p. 699-711.
728 22. S, M., et al., *Extracellular signal-regulated kinases phosphorylate mitogen-activated*
729 *protein kinase phosphatase 3/DUSP6 at serines 159 and 197, two sites critical for its*
730 *proteasomal degradation - PubMed.* Molecular and cellular biology, 2005 Jan. **25**(2).
731 23. Ruckert, M.T., et al., *Protein tyrosine phosphatases: promising targets in pancreatic*
732 *ductal adenocarcinoma.* Cell Mol Life Sci, 2019. **76**(13): p. 2571-2592.
733 24. Furukawa, T., et al., *Potential tumor suppressive pathway involving DUSP6/MKP-3 in*
734 *pancreatic cancer.* Am J Pathol, 2003. **162**(6): p. 1807-15.
735 25. Xu, S., et al., *Abrogation of DUSP6 by hypermethylation in human pancreatic cancer.*
736 J Hum Genet, 2005. **50**(4): p. 159-167.

737 26. Nagathihalli, N.S., et al., *STAT3 Mediated Remodeling of the Tumor Microenvironment*
738 *Results in Enhanced Tumor Drug Delivery in a Mouse Model of Pancreatic Cancer.*
739 Gastroenterology, 2015 Aug 7. **149**(7).
740 27. Bankhead, P., et al., *QuPath: Open source software for digital pathology image*
741 *analysis.* Scientific Reports 2017 7:1, 2017-12-04. **7**(1).
742 28. Yi, Z., et al., *KDM6A Regulates Cell Plasticity and Pancreatic Cancer Progression by*
743 *Noncanonical Activin Pathway.* Cellular and Molecular Gastroenterology and
744 Hepatology, 2022/01/01. **13**(2).
745 29. S, Y., et al., *A Novel MIF Signaling Pathway Drives the Malignant Character of*
746 *Pancreatic Cancer by Targeting NR3C2 - PubMed.* Cancer research, 07/01/2016.
747 **76**(13).
748 30. G, Z., et al., *DPEP1 inhibits tumor cell invasiveness, enhances chemosensitivity and*
749 *predicts clinical outcome in pancreatic ductal adenocarcinoma - PubMed.* PloS one,
750 2012. **7**(2).
751 31. Badea, L., et al., *Combined gene expression analysis of whole-tissue and*
752 *microdissected pancreatic ductal adenocarcinoma identifies genes specifically*
753 *overexpressed in tumor epithelia.* Hepatogastroenterology, 2008. **55**(Nov-Dec): p. 11.
754 32. Moffitt, R.A., et al., *Virtual microdissection identifies distinct tumor- and stroma-*
755 *specific subtypes of pancreatic ductal adenocarcinoma.* Nature Genetics 2015 47:10,
756 2015-09-07. **47**(10).
757 33. Y, O., et al., *SERPINB3-MYC axis induces the basal-like/squamous subtype and*
758 *enhances disease progression in pancreatic cancer - PubMed.* Cell reports, 12/26/2023.
759 **42**(12).
760 34. C, M., et al., *Experimental microdissection enables functional harmonisation of*
761 *pancreatic cancer subtypes - PubMed.* Gut, 2019 Jun. **68**(6).
762 35. Bailey, P., et al., *Genomic analyses identify molecular subtypes of pancreatic cancer.*
763 Nature, 2016. **531**(7592): p. 47-52.
764 36. Jin, X., et al., *A metastasis map of human cancer cell lines.* Nature, 2020 Dec 9.
765 **588**(7837).
766 37. A, S., et al., *Gene set enrichment analysis: a knowledge-based approach for*
767 *interpreting genome-wide expression profiles - PubMed.* Proceedings of the National
768 Academy of Sciences of the United States of America, 10/25/2005. **102**(43).

38. Carpenter, E.S., et al., *Analysis of Donor Pancreata Defines the Transcriptomic Signature and Microenvironment of Early Neoplastic Lesions.* Cancer Discovery, 2023/06/06. **13**(6).
39. Collisson, E.A., et al., *Subtypes of pancreatic ductal adenocarcinoma and their differing responses to therapy.* Nature Medicine 2011 17:4, 2011-04-03. **17**(4).
40. Bojmar, L., et al., *Multi-parametric atlas of the pre-metastatic liver for prediction of metastatic outcome in early-stage pancreatic cancer.* Nature Medicine 2024 30:8, 2024-06-28. **30**(8).
41. Birnbaum, D.J., et al., *Validation and comparison of the molecular classifications of pancreatic carcinomas.* Mol Cancer, 2017. **16**(1): p. 168.
42. Kidger, A.M., et al., *Suppression of mutant Kirsten-RAS (KRAS(G12D))-driven pancreatic carcinogenesis by dual-specificity MAP kinase phosphatases 5 and 6.* Oncogene, 2022. **41**(20): p. 2811-2823.
43. Kato, M., et al., *Dual-specificity phosphatase 6 plays a critical role in the maintenance of a cancer stem-like cell phenotype in human endometrial cancer.* Int J Cancer, 2020. **147**(7): p. 1987-1999.
44. Wu, F., et al., *Nuclear-Biased DUSP6 Expression is Associated with Cancer Spreading Including Brain Metastasis in Triple-Negative Breast Cancer.* International Journal of Molecular Sciences, 2019/06. **20**(12).
45. Wu, Q.N., et al., *Pharmacological inhibition of DUSP6 suppresses gastric cancer growth and metastasis and overcomes cisplatin resistance.* Cancer Lett, 2018. **412**: p. 243-255.
46. Timofeev, O., et al., *ERK pathway agonism for cancer therapy: evidence, insights, and a target discovery framework.* npj Precision Oncology 2024 8:1, 2024-03-14. **8**(1).
47. Gutierrez-Prat, N., et al., *DUSP4 protects BRAF- and NRAS-mutant melanoma from oncogene overdose through modulation of MITF.* Life Science Alliance, 2022 May 17. **5**(9).
48. Bulle, A., et al., *Combined KRAS-MAPK pathway inhibitors and HER2-directed drug conjugate is efficacious in pancreatic cancer.* Nature Communications 2024 15:1, 2024-03-20. **15**(1).
49. T, I., et al., *Paralog knockout profiling identifies DUSP4 and DUSP6 as a digenic dependence in MAPK pathway-driven cancers - PubMed.* Nature genetics, 2021 Dec. **53**(12).

802 50. Daemen, A., et al., *Metabolite profiling stratifies pancreatic ductal adenocarcinomas*
803 *into subtypes with distinct sensitivities to metabolic inhibitors.* Proceedings of the
804 National Academy of Sciences of the United States of America, 2015/08/08. **112**(32).
805 51. Hsu, W.-C., et al., *DUSP6 mediates T cell receptor-engaged glycolysis and restrains*
806 *TFH cell differentiation.* Proceedings of the National Academy of Sciences, 2018-8-21.
807 **115**(34).
808 52. Li, M., et al., *Biological role of metabolic reprogramming of cancer cells during*
809 *epithelial-mesenchymal transition (Review).* Oncology Reports, 2019-02-01. **41**(2).
810 53. Kang, H., et al., *Role of Metabolic Reprogramming in Epithelial–Mesenchymal*
811 *Transition (EMT).* International Journal of Molecular Sciences, 2019/04. **20**(8).
812 54. Joshi, V.B., O.L.G. Ruiz, and G.L. Razidlo, *The Cell Biology of Metastatic Invasion in*
813 *Pancreatic Cancer: Updates and Mechanistic Insights.* Cancers, 2023/04. **15**(7).

# Figure 1

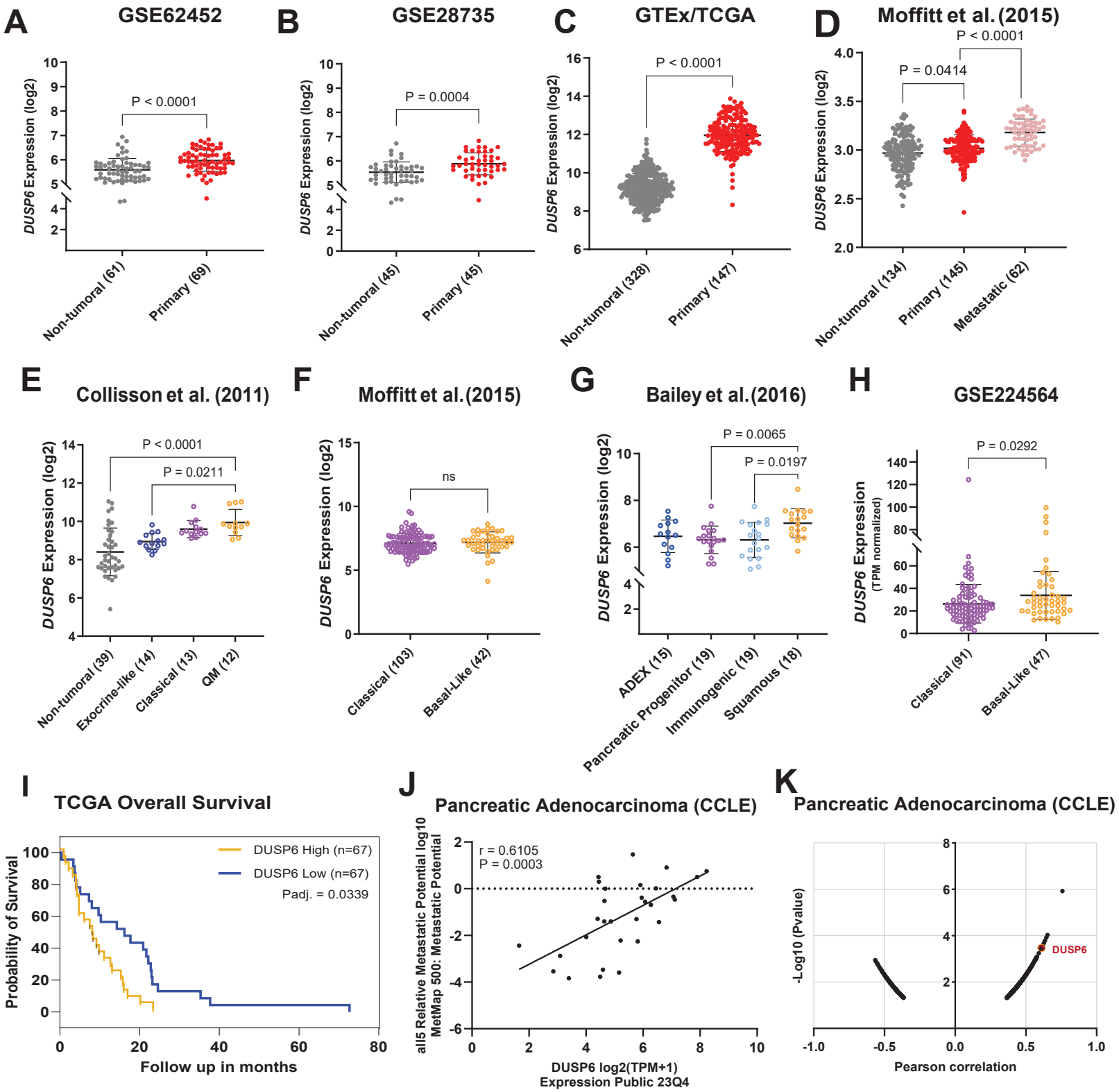
A
GSE62452
DUSP6 Expression (log2)
P < 0.0001
Non-tumoral (61)
Primary (69)
B
GSE28735
DUSP6 Expression (log2)
P = 0.0004
Non-tumoral (45)
Primary (45)
C
GTEx/TCGA
DUSP6 Expression (log2)
P < 0.0001
Non-tumoral (328)
Primary (147)
D
Moffitt et al.(2015)
DUSP6 Expression (log2)
P < 0.0001
P = 0.0414
Non-tumoral (134)
Primary (145)
Metastatic (62)
E
Collisson et al. (2011)
DUSP6 Expression (log2)
P < 0.0001
P = 0.0211
Non-tumoral (39)
Exocrine-like (14)
Classical (13)
QM (12)
F
Moffitt et al.(2015)
DUSP6 Expression (log2)
ns
Classical (103)
Basal-Like (42)
G
Bailey et al.(2016)
DUSP6 Expression (log2)
P = 0.0065
P = 0.0197
ADEX (15)
Pancreatic Progenitor (19)
Immunogenic (19)
Squamous (18)
H
GSE224564
DUSP6 Expression
(TPM normalized)
P = 0.0292
Classical (91)
Basal-Like (47)
I
TCGA Overall Survival
Probability of Survival
DUSP6 High (n=67)
DUSP6 Low (n=67)
Padj. = 0.0339
Follow up in months
J
Pancreatic Adenocarcinoma (CCLE)
all5 Relative Metastatic Potential log10
MetMap 500: Metastatic Potential
r = 0.6105
P = 0.0003
DUSP6 log2(TPM+1)
Expression Public 23Q4
K
Pancreatic Adenocarcinoma (CCLE)
-Log10 (Pvalue)
DUSP6
Pearson correlation

# Figure 2

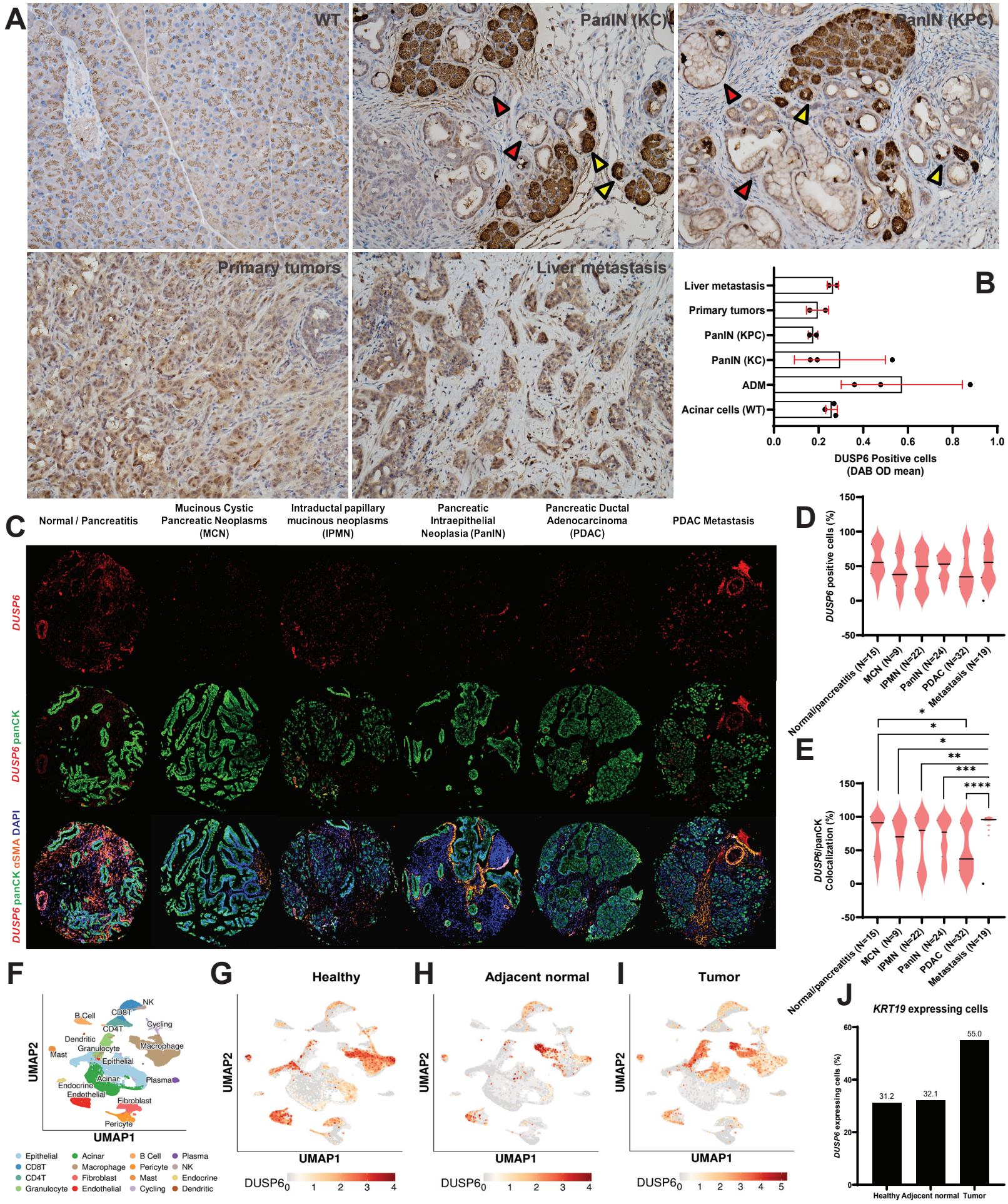
A
WT
PanIN (KC)
PanIN (KPC)
Primary tumors
Liver metastasis
B
Liver metastasis
Primary tumors
PanIN (KPC)
PanIN (KC)
ADM
Acinar cells (WT)
0.0
0.2
0.4
0.6
0.8
1.0
DUSP6 Positive cells
(DAB OD mean)
C
Normal / Pancreatitis
Mucinous Cystic Pancreatic Neoplasms (MCN)
Intraductal papillary mucinous neoplasms (IPMN)
Pancreatic Intraepithelial Neoplasia (PanIN)
Pancreatic Ductal Adenocarcinoma (PDAC)
PDAC Metastasis
DUSP6
DUSP6 panCK
DUSP6 panCK αSMA DAPI
D
DUSP6 positive cells (%)
150
100
50
0
-50
Normal/pancreatitis (N=15)
MCN (N=9)
IPMN (N=22)
PanIN (N=24)
PDAC (N=32)
Metastasis (N=19)
E
DUSP6/panCK Colocalization (%)
*
**
***
****
F
UMAP2
UMAP1
NK
B Cell
CD8T
CD4T
Cycling
Dendritic
Granulocyte
Macrophage
Mast
Epithelial
Acinar
Plasma
Endocrine
Endothelial
Fibroblast
Pericyte
Epithelial
CD8T
CD4T
Granulocyte
Acinar
Macrophage
Fibroblast
Endothelial
B Cell
Pericyte
Mast
Cycling
Plasma
NK
Endocrine
Dendritic
G
Healthy
H
Adjacent normal
I
Tumor
DUSP6
0
1
2
3
4
5
J
KRT19 expressing cells
DUSP6 expressing cells (%)
60
40
20
0
31.2
32.1
55.0
Healthy
Adjecent normal
Tumor

# Figure 3

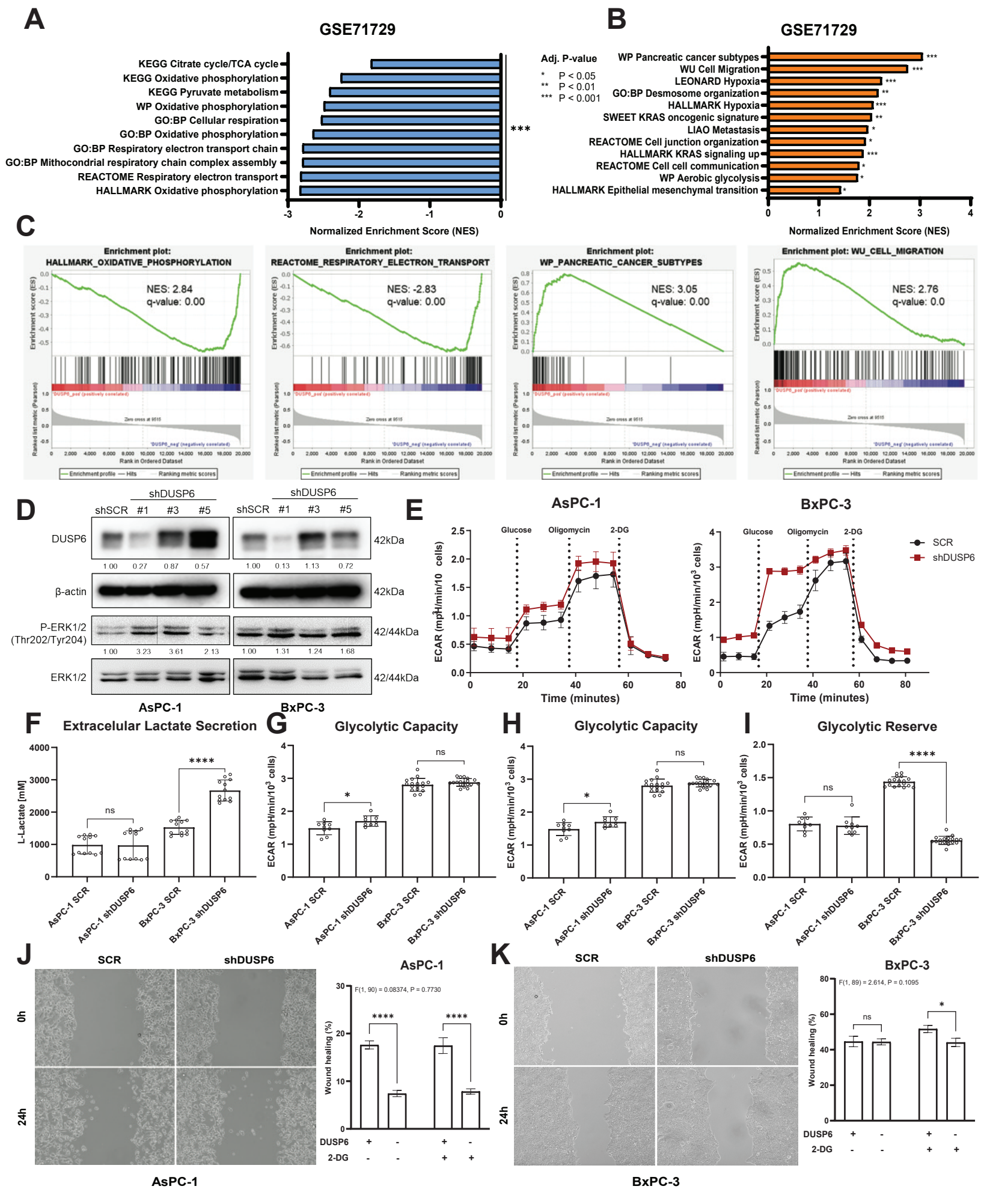
A
GSE71729
KEGG Citrate cycle/TCA cycle
KEGG Oxidative phosphorylation
KEGG Pyruvate metabolism
WP Oxidative phosphorylation
GO:BP Cellular respiration
GO:BP Oxidative phosphorylation
GO:BP Respiratory electron transport chain
GO:BP Mithocondrial respiratory chain complex assembly
REACTOME Respiratory electron transport
HALLMARK Oxidative phosphorylation
***
-3
-2
-1
0
Normalized Enrichment Score (NES)
B
GSE71729
Adj. P-value
* P < 0.05
** P < 0.01
*** P < 0.001
WP Pancreatic cancer subtypes
WU Cell Migration
LEONARD Hypoxia
GO:BP Desmosome organization
HALLMARK Hypoxia
SWEET KRAS oncogenic signature
LIAO Metastasis
REACTOME Cell junction organization
HALLMARK KRAS signaling up
REACTOME Cell cell communication
WP Aerobic glycolysis
HALLMARK Epithelial mesenchymal transition
0
1
2
3
4
Normalized Enrichment Score (NES)
C
Enrichment plot: HALLMARK_OXIDATIVE_PHOSPHORYLATION
NES: 2.84
q-value: 0.00
Enrichment plot: REACTOME_RESPIRATORY_ELECTRON_TRANSPORT
NES: -2.83
q-value: 0.00
Enrichment plot: WP_PANCREATIC_CANCER_SUBTYPES
NES: 3.05
q-value: 0.00
Enrichment plot: WU_CELL_MIGRATION
NES: 2.76
q-value: 0.0
Rank in Ordered Dataset
Enrichment profile
Hits
Ranking metric scores
D
shSCR
shDUSP6
#1
#3
#5
DUSP6
β-actin
P-ERK1/2 (Thr202/Tyr204)
ERK1/2
42kDa
42/44kDa
1.00 0.27 0.87 0.57
1.00 0.13 1.13 0.72
1.00 3.23 3.61 2.13
1.00 1.31 1.24 1.68
AsPC-1
BxPC-3
E
AsPC-1
BxPC-3
Glucose
Oligomycin
2-DG
SCR
shDUSP6
ECAR (mpH/min/10 cells)
ECAR (mpH/min/10^3 cells)
Time (minutes)
F
Extracelular Lactate Secretion
L-Lactate [mM]
ns
****
G
Glycolytic Capacity
ECAR (mpH/min/10^3 cells)
*
ns
H
Glycolytic Capacity
*
ns
I
Glycolytic Reserve
ns
****
AsPC-1 SCR
AsPC-1 shDUSP6
BxPC-3 SCR
BxPC-3 shDUSP6
J
SCR
shDUSP6
0h
24h
AsPC-1
F(1, 90) = 0.08374, P = 0.7730
Wound healing (%)
****
****
DUSP6
2-DG
K
SCR
shDUSP6
0h
24h
BxPC-3
F(1, 89) = 2.614, P = 0.1095
Wound healing (%)
ns
*
DUSP6
2-DG

**Figure 1 – *DUSP6* overexpression is correlated to tumor metastatic potential and worse prognosis.** *In silico* datasets from GSE62452 [29] **(A)**, GSE28735 [30] **(B)** and GTex/TCGA **(C)** assessing *DUSP6*'s differential expression between non-tumoral pancreatic tissue and primary tumor tissue; **(D)** GSE71729 [32] assessing *DUSP6* expression between non-tumoral pancreatic tissue, primary and metastatic tumor tissue; *In silico* gene expression analysis utilizing **(E)** Collisson [39], **(F)** Moffitt [32], **(G)** Bailey [35] and **(H)** GSE224564 [33] datasets to assess *DUSP6* expression among PDAC molecular subtypes; **(I)** Kaplan-Meier (Log-rank) plot comparing *DUSP6* expression and patients' overall survival using the TCGA dataset. Padj. = 0.0339, N = 67 for each group; **(J & K)** Pearson correlation analysis between *DUSP6* expression in CCLE PDAC cell lines and their metastatic potential (MetMap 500 [36]). R = 0.6105, P = 0.0003. ADEX: aberrantly differentiated endocrine–exocrine; QM: quasi-mesenchymal. (A, H) Mann-Whitney unpaired test. (B, C, F) Welch's unpaired t-test. (D, G) Brown-Forsythe and Welch unpaired ANOVA test. (E) Kruskal-Wallis unpaired test. * P < 0.05; ** P < 0.01; *** P < 0.001; **** P < 0.0001.

**Figure 2 – *DUSP6* is upregulated in PDAC epithelial cells in human and mouse tissue. (A)** DUSP6 immunohistochemistry staining (20x magnification) in wild type (WT) pancreatic tissue (N=3), KC (N=3) and KPC (N=6) mice. Yellow arrows indicate acinar-to-ductal metaplasia (ADM) lesions and red arrows indicate Pancreatic Intraepithelial Neoplasia (PanIN) lesions. Quantification (B) shows DAB OD mean ± SD in DUSP6 positive cells from 10 randomly selected areas in each slide stratified by lesion grade; **C)** Multiplex *in situ* hybridization with *DUSP6* (red, RNAscope), panCK (green), αSMA (orange) and DAPI (blue). Images are representative of normal pancreatic tissue/pancreatitis, Intraductal papillary mucinous neoplasms (IPMN), Mucinous Cystic Pancreatic Neoplasms (MCN), Pancreatic Intraepithelial Neoplasia (PanIN), Pancreatic Ductal Adenocarcinoma (PDAC) and PDAC metastasis samples composed from 2 human TMA sections; **D)** Quantification of the percentage *DUSP6* positive cells normalized by total number of cells in each TMA core; **E)** Quantification of the percentage of cells that are positive for both *DUSP6* and panCK, normalized by total number of cells in each TMA core. Welch's unpaired t-test; **F)** UMAP plot of all cells captured from single-cell RNA sequencing of eleven human tumor samples [28]. Cell types are identified by color. Following UMAPs show DUSP6 expression among cell types in healthy pancreatic tissue **(G)**, adjacent normal pancreatic tissue **(H)** and

PDAC samples **(I)**; **J)** Percentage of cells co-expressing *DUSP6* and *KRT19* (epithelial marker) in healthy pancreatic tissue, adjacent normal pancreatic tissue and PDAC samples assessed by single-cell RNA-seq [28]. * P < 0.05; ** P < 0.01; *** P < 0.001; **** P < 0.0001.

**Figure 3 – DUSP6 downregulation increases glycolysis in PDAC cell lines, but glycolysis inhibition does not rescue migratory phenotype.** GSEA analysis of GSE71729 dataset showing pathways significantly negatively **(A & C)** and positively **(B & C)** correlated to *DUSP6* expression in metastatic samples; **D)** Western blot analysis of DUSP6 expression and ERK1/2 phosphorylation upon DUSP6 knockdown. Quantification shows DUSP6 expression normalized to β-actin, and P-ERK1/2 normalized to total ERK1/2 levels; **E)** Representative curves of extracellular acidification rates (ECAR) measured in AsPC-1 and BxPC-3 with sequential injections of glucose (10 mM), oligomycin (1 µM) and 2-DG (100 mM), respectively in a Seahorse assay; **F)** Basal extracellular lactate secretion levels upon DUSP6 knockdown in complete media; **G)** Basal glycolysis corresponds to glycolytic levels under basal conditions, no stimulation; **H)** Glycolytic capacity is measured after inhibition of ATP synthase (complex V of the mitochondrial respiratory chain); **I)** Glycolytic reserve corresponds to the difference between glycolytic capacity and basal glycolysis. Assessment of migratory capacity upon 2-DG treatment in AsPC-1 **(J)** and BxPC-3 **(K)** upon DUSP6 knockdown. Seahorse Glycolysis Stress Test was performed in 9-12 replicates in 2 independent experiments. Results represent mean ± SD of one representative experiment. L-Lactate assay was performed in 2 independent experiments with 6 replicates each. Results represent mean ± SEM. Welch's unpaired t-test; Migration graphs show 3 independent experiments with 4-6 replicates each. Results represent mean ± SEM. Mixed-effects analysis with Šídák's multiple comparisons test. *ns*: not significant; * P < 0.05; ** P < 0.01; *** P < 0.001; **** P < 0.0001.